Reaction Mechanism between Carbonyl Oxide and Hydroxyl Radical: A Theoretical Study

Alex Mansergas and Josep M. Anglada*

Theoretical and Computational Chemistry Group, Departament de Química Orgànica Biològica, Institut d'Investigacions Químiques i Ambientals de Barcelona, IIQAB − CSIC, c/ Jordi Girona 18, E-08034 Barcelona, Spain

Received: December 7, 2005; In Final Form: January 31, 2006

The reaction mechanism of carbonyl oxide with hydroxyl radical was investigated by using CASSCF, B3LYP, QCISD, CASPT2, and CCSD(T) theoretical approaches with the 6-311+G(d,p), 6-311+G(2df, 2p), and aug-cc-pVTZ basis sets. This reaction involves the formation of $H_2CO + HO_2$ radical in a process that is computed to be exothermic by 57 kcal/mol. However, the reaction mechanism is very complex and begins with the formation of a pre-reactive hydrogen-bonded complex and follows by the addition of HO radical to the carbon atom of H_2COO, forming the intermediate peroxy-radical $H_2C(OO)OH$ before producing formaldehyde and hydroperoxy radical. Our calculations predict that both the pre-reactive hydrogen-bonded complex and the transition state of the addition process lie energetically below the enthalpy of the separate reactants (ΔH(298K) = −6.1 and −2.5 kcal/mol, respectively) and the formation of the $H_2C(OO)OH$ adduct is exothermic by about 74 kcal/mol. Beyond this addition process, further reaction mechanisms have also been investigated, which involve the abstraction of a hydrogen of carbonyl oxide by HO radical, but the computed activation barriers suggest that they will not contribute to the gas-phase reaction of $H_2COO + HO$.

I. Introduction

Carbonyl oxide (H_2COO) and hydroxyl radical (HO) are important species in the atmosphere.[1] Hydroxyl radical is among the most important oxidants in the troposphere. It oxidizes the atmospheric volatile organic compounds (VOC), which are involved in the conversion of NO to NO_2 and triggers the atmospheric ozone production.[1] HO radical is formed mainly by photolysis of ozone in daytime or by reaction between nitric oxide with aldehydes or alkenes, followed by reaction with O_2 at nighttime.[1] However, there is recent experimental and theoretical evidence that the reaction of ozone with alkenes constitutes also a non-photochemical source of HO radicals that operates at nighttime as well as in daytime.[2−16]

Carbonyl oxide is formed in the reaction of ozone with unsaturated hydrocarbons. The alkene ozonolysis follows the so-called Criegee mechanism[17] and is initiated with a 1,3-cycloaddition of ozone across the double bond forming the 1,2,3-trioxolane or primary ozonide (POZ), which decomposes, producing a carbonyl oxide (or Criegee intermediate) and a carbonyl compound (reaction 1).

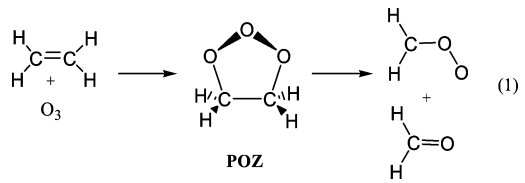

(1)

The atmospheric importance of carbonyl oxide's chemistry is evident if one takes into account that the release of unsaturated hydrocarbons to the atmosphere such as ethene, propene, or isoprene is larger than 500×10^9 kg C/yr[1] and its reaction with ozone constitutes one of its main degradation paths. In the gas phase, reaction 1 is highly exothermic so that carbonyl oxides are formed with an excess of vibrational energy and may decompose unimolecularly (among 37−50%) or may become collisionally stabilized (among 63−50%).[18−22] The gas-phase unimolecular decomposition of carbonyl oxide produces HCOOH, CO_2, CO, H_2O, H_2, H, HCO, HO, H_2CO, and O and the corresponding mechanisms have been investigated recently.[8,21,23−32] The stabilized Criegee intermediates can react with other atmospheric species such as NO_x, SO_2, aldehydes, organic acids, HO_x, or water vapor and can contribute to the formation of aerosols.[33−40]

In this paper we report a high level theoretical study on the reaction mechanism of carbonyl oxide with hydroxyl radical. In this investigation we have considered the processes schematized by reactions 2−4 below, which include the addition of hydroxyl radical to carbonyl oxide (reaction 2), the hydrogen abstraction by HO (reaction 3), and a hydrogen atom migration from the carbon to the terminal oxygen of carbonyl oxide, which is assisted by HO radical (reaction 4).

$$H_2COO + HO \rightarrow H_2C(OO)OH \rightarrow H_2CO + HO_2 \quad (2)$$

$$H_2COO + HO \rightarrow HCOO + H_2O \quad (3)$$

$$H_2COO + HO \rightarrow HC(OOH) + HO \rightarrow HCO + 2HO \quad (4)$$

As far as we know, this is the first study on the $H_2COO + HO$ reaction. The importance of this reaction may be limited for atmospheric purposes because of the competition of the reaction of carbonyl oxide with water vapor, which is in higher concentration in the troposphere. However, we believe that this reaction has a high mechanistic interest, as it involves the interaction of a biradical (H_2COO) with a radical (HO). Thus, an accurate knowledge of its reaction mechanism is very

* To whom correspondence should be addressed. E-mail: anglada@iiqab.csic.es.

10.1021/jp057133x CCC: $33.50
Published on Web 03/01/2006

valuable for the study of other reactions of atmospheric interest involving biradical and radical species such as ozone plus hydroxyl radical or carbonyl oxide or ozone plus nitrogen oxides.[41]

II. Technical Details

The reaction considered in the present work involves the interaction of a molecule with a certain degree of biradical character (H_2COO) with a radical (HO). Therefore, and from a technical point of view, it is necessary to use theoretical approaches capable of considering structures whose electronic configuration possesses an important degree of multireferential character. Thus, in a first step, we have employed the complete active space self-consistent field (CASSCF) method[42] using both the 6-31G(d,p)[43] and 6-311+G(2df,2p)[44,45] basis sets to optimize and characterize all stationary points along the potential energy surface. At the CASSCF/6-311+G(2df,2p) level of treatment we have also performed harmonic vibrational frequency calculations to ensure the nature of the stationary points (minima or transition states) and to calculate the ZPE and the contributions of the enthalpy and free energy. The active space for the CASSCF calculations of a given structure has been chosen according to the fractional occupation of the natural orbitals (NO's)[46] generated from a first-order density matrix of a MRD-CI wave function,[47−49] which is based on the correlation of all valence electrons. In general, we have used an active space consisting of 11 electrons over 10 orbitals, which form a CASSCF space of 27720 configuration state functions (CSFs) in C_1 symmetry. The effect of dynamic valence electron correlation was considered by performing CASPT2 single-point calculations based on a common CASSCF(17,14) reference function, forming a CASSCF space of 2576574 CSFs in C_1 symmetry. The latter was chosen because the (17,14) active space corresponds to the sum of the appropriate active spaces describing H_2COO (12,9) and HO (5,5). A schematic description of the active space composition in the CASSCF calculations is also reported as Supporting Information.

To check the behavior of single-determinant based methods regarding the geometries and relative energies of the stationary points, we have carried out additional calculations that are detailed as follows:

In a second step we employed DFT with the hybrid functional B3LYP[50] and the 6-311+G(2df,2p) basis set to optimize and characterize all stationary points in the potential energy surface as minima or saddle point. At this level of theory we have verified the connectivity between a given transition state (TS) with the corresponding reactant and product by performing intrinsic reaction coordinate (IRC)[51−53] calculations. In a third step all stationary points were also optimized and characterized at QCISD level of theory,[54] employing the 6-311+G(d,p) basis set.[44,45] In both cases, the harmonic vibrational calculations have been used to calculate the ZPE and the contributions of the enthalpy and free energy. Moreover, to obtain more reliable energy values, at the B3LYP/6-311+G(2df,2p) and QCISD/6-311+G(d,p) optimized geometries, we also performed single-point CCSD(T)[55−58] energy calculations using the aug-cc-pVTZ basis set.[59,60] In these calculations we took into account the value of the T_1 diagnostic[61,62] in the CCSD wave function in order to assess the reliability of these calculations with regard to a possible multireference character of the wave function at the corresponding stationary point. Thus, following Rienstra-Kiracofe,[62] CCSD wave functions having a T_1 diagnostic larger than 0.044 are expected not to be reliable. In addition, the basis set superposition error (BSSE) according to the counterpoise method by Boys and Bernardi[63] was also calculated at this level of theory for all the complexes.

The quantum chemical calculations were carried out using the Gaussian,[64] GAMESS,[65] Molcas,[66] and MRD-CI program packages. The Molden program[67] was also used to visualize the geometric and electronic features of the different stationary points.

Finally, and for some stationary points of interest, we also analyzed the bonding features according to the Atoms in Molecules (AIM) theory by Bader.[68] This analysis was carried out over the first-order density matrix obtained at the QCISD and CASSCF levels of theory, by using the AIMPAC program package.[69]

III. Results and Discussion

Throughout the text, the structures of the stationary points are designated by **C** for the hydrogen-bonded complexes that are minima on the potential energy surface, by **TS** for the transition states, and by **M** for the minima in the potential energy surface. In addition, we have appended the numbers 1, 2, 3, etc., to each structure acronym in order to differentiate the stationary points along the reaction path. The relevant geometrical parameters of all stationary points are displayed in Figures 1, 3, and 5. The relative energies, enthalpies, Gibbs free energies, ZPVE, and imaginary frequencies of the corresponding stationary points are summarized in Table 1. Figure 2 shows a schematic reaction enthalpy profile. Table 2 contains absolute and relative energy values for the hydrogen-bonded complex **C1** and the transition state **TS1** according to calculations carried out at different levels of theory, while Figure 4 displays the natural orbitals of the CASSCF wave function describing the addition of hydroxyl radical to carbonyl oxide. The full set of results (namely, the Cartesian coordinates of all stationary points, the absolute energies, and the AIM topological parameters at the bond critical points (bcp) computed for several stationary points of interest) is given in the Supporting Information. In what follows, and unless otherwise stated, the geometries and energies obtained at CASSCF and CASPT2 levels of theory will be discussed in the text.

Reactants and Products. The calculated geometries of the reactants and products of reactions 2, 3, and 4 (Figure 1) compare well with other results published previously in the literature.[26,29,31,70−74] The most significant differences are in the HCOO products. An *anti*-HCOO (C_S, $^2A'$) radical was reported recently by Huang and co-workers,[74] in connection with a theoretical study on the combustion of CH. Our calculations predict an *anti*-HCOO radical to have a structure similar to that of its precursor carbonyl oxide (with a $d(CO) = 1.224$ Å, $d(OO) = 1.351$ Å, and a COO angle $= 121.5°$; see Figure 1), whereas Huang and co-workers report a much larger O···O length (1.586 Å), a shorter C···O bond distance (1.200 Å), and a smaller COO angle (97.6°).[74] However, additional calculations indicate that the structure computed in this work and that reported by Huang and co-workers correspond to different electronic states, although both are of symmetry $^2A'$.[41] On the other side, the *syn*-HCOO radical (C_S, $^2A'$) was not reported previously in the literature.

From an electronic point of view, it is worth here to remind the reader that the gas-phase H_2COO is mainly described by the electronic configurations [0.94 (...10a′^{2}1a″^{2}2a″^{2}) − 0.20 (...10a′^{2}1a″^{2}3a″^{2})], having a certain amount of biradical character.[73] The a″ orbitals are π orbitals and therefore carbonyl oxide constitutes a system with four π electrons, which play a key role in its reactivity.

TABLE 1: Imaginary Frequencies (Imag, in cm^{-1}), Zero-Point Energies (ZPE in kcal/mol), Entropies (*S* in e.u.), and Reaction and Activation Energies, Enthalpies, and Free Energies (ΔE, ΔH(298K) and ΔG(298K) in kcal/mol) for the Reaction between H_2COO and HO[a]

compound	M[b]	Imag	ZPE	S	ΔE[c]	ΔE + ZPE[c]	ΔH[c]	ΔG[c]
H_2COO + HO	B		24.8	102.1	0.00	0.00	0.00	0.00
	Q		24.9	102.3	0.00	0.00	0.00	0.00
	C		25.1	102.3	0.00	0.00	0.00	0.00
C1 (C_s, ^2A)	B		26.6	78.3	−7.19	−5.75	−6.23	0.86
					(−6.56)	(−5.12)	(−5.60)	(1.49)
	Q		26.7	78.9	−8.15	−6.28	−6.72	0.25
					(−7.52)	(−5.65)	(−6.09)	(0.88)
	C		26.9	80.5	−5.84	−4.01	−4.32	2.17
					(−5.21)	(−3.38)	(−3.69)	(2.80)
	C′		26.7	78.9	−6.56	−4.69	−5.13	1.84
					(−5.93)	(−4.06)	(−4.50)	(2.47)
TS1 (C_1, ^2A)	B	−216.8	26.6	70.6	−5.80	−4.09	−5.25	4.14
	Q	−360.7	26.9	72.4	−4.70	−2.63	−3.60	5.29
	C	−832.9	26.3	75.0	−6.70	−5.50	−6.21	1.90
	C′	−360.7	26.9	72.4	−3.64	−1.57	−2.54	6.35
M1 (C_1, ^2A)	B		30.4	69.6	−78.22	−72.65	−73.95	−64.25
	Q		30.4	69.6	−78.09	−72.53	−73.85	−64.11
	C		31.8	68.9	−78.18	−71.50	−72.91	−62.95
TS8 (C_s, ^2A)	B	−806.9	26.6	67.4	−61.25	−59.47	−61.06	−50.70
	Q				−60.96	−59.20	−60.81	−50.40
C3 (C_s, ^2A)	B		27.6	76.1	−65.71	−62.91	−63.40	−55.62
	Q				−65.40	−62.62	−63.12	−55.30
H_2CO + HO_2	B		25.6	108.3	−57.89	−57.21	−57.15	−58.98
	Q		25.7	108.3	−57.74	−56.93	−57.04	−58.82
C2 (C_1, ^2A)	B		26.7	77.0	−5.71	−3.83	−4.42	2.82
					(−5.00)	(−3.12)	(−3.71)	(3.53)
TS2 (C_s, ^2A)	B	−1517.7	23.1	71.8	5.39	3.68	2.71	11.77
	Q	−2005.1	24.1	72.2	4.87	4.06	3.10	12.07
	C	−2869.7	23.6	72.5	4.95	3.50	2.59	11.47
TS3 (C_1, ^2A)	B	−1424.2	24.0	73.7	10.69	9.87	9.07	17.55
	Q	−1510.3	25.6	70.6	7.58	8.34	7.19	16.64
	C	−1733.3	26.5	70.5	9.57	10.95	9.77	19.25
TS4 (C_1, ^2A)	B	−1469.9	24.5	70.0	6.15	5.82	4.65	14.23
	Q	−1993.4	25.1	69.5	5.84	6.04	4.79	14.55
	C	−2749.6	25.6	69.6	5.31	5.79	4.53	14.27
***a*-HCOO + H_2O**	B		24.0	105.4	−2.62	−3.43	−3.08	−4.06
	Q		25.6	105.3	−3.31	−2.53	−2.26	− 3.16
	C		24.6	105.9	−6.37	−6.80	−6.52	− 7.61
TS5 (C_1, ^2A)	B	−1473.1	23.7	74.5	11.96	10.77	10.05	18.28
	Q	−1483.5	25.6	70.8	6.36	7.12	5.97	15.36
	C	−1705.1	26.5	70.6	8.54	9.97	8.80	18.23
TS6 (C_1, ^2A)	B	−1466.4	23.5	74.9	13.28	11.96	11.29	19.40
	Q	−1482.2	25.7	70.7	6.88	7.71	6.54	15.96
	C	−1730.2	26.4	70.6	8.80	10.13	8.96	18.40
***s*-HCOO + H_2O**	Q		24.4	106.8	−9.97	−10.43	−10.00	−11.35
	C		24.5	106.4	1.65	1.07	1.44	0.19
TS7 (C_s, ^2A)	B	−1221.0	22.4	67.5	19.85	17.38	15.75	26.07
	Q	−1441.7	23.5	69.0	19.26	17.87	16.43	26.35
	C	−1428.1	25.4	68.9	17.04	17.32	15.84	25.80
HCO + 2HO	B		18.7	138.8	−4.06	−10.14	−8.33	−19.24
	Q		18.9	138.7	−3.88	−9.88	− 8.02	−18.89
	C		19.2	137.3	−3.59	−9.59	− 7.66	−18.10

[a] The Imag, ZPE, *S*, and the contribution to enthalpy and free energy according to results obtained at B = B3LYP/6-311+G(2df,2p); Q, C′ = QCISD/6-311+G(d,p); and C = CASSCF(11,10)/6-311+G(2df,2p) levels of theory. [b] The relative energies (ΔE) are computed at: B = CCSD(T)/aug-cc-pVTZ//B3LYP/ 6-311+G(2df,2p); Q = CCSD(T)/aug-cc-pVTZ//QCISD/6-311+G(d,p); C = CASPT2(17,14)/6-311+G(2df,2p)//CASSCF(11,10)/6-311+G(2df,2p); and C′ = CASPT2(17,14)/6-311+G(2df,2p)//QCISD/6-311+G(d,p) levels of theory, respectively, while the relative enthalpies (ΔH) and Gibbs free energies (ΔG) are computed by adding to ΔE the corrections obtained at B, Q, or C and C′ levels of theory, respectively. [c] Values in parentheses include BSSE corrections computed at CCSD(T)/aug-cc-pvtz//QCISD/6-311+G(d,p) level of theory.

With regard to the reaction energetic, Table 1 shows that the formation of H_2CO and HO_2 radical (reaction 2) is computed to be exothermic by 57.0 kcal/mol; the formation of HCO plus 2 HO radicals (reaction 4) is computed to be exothermic by about 8 kcal/mol, whereas the formation of *syn*- and *anti*-HCOO plus H_2O (reaction 3) are computed to be endothermic by 1.44 kcal/mol and exothermic by 6.52 kcal/mol, respectively, at CASPT2 level of theory. The results displayed in Table 1

TABLE 2: Single-Point CCSD(T)/aug-cc-pVTZ and CASPT2(17,14)/6-311+G(2df,2p) Absolute Energies (in hartree), Relative Stabilization Energies (Values in Parentheses, in kcal/mol), and ΔE (TS1−C1) in kcal/mol, Obtained at the Corresponding Stationary Points Computed at Different Levels of Theory

	CCSD(T)/aug-cc-pVTZ					CASPT2(17,14)/6-311+G(2df,2p)				
geometry[a]	**C1**[b]		**TS1**[c]		Δ*E*	C1		TS1		Δ*E*
Q	−264.99047	(0.00)	−264.98497	(0.00)	3.45	−264.91251	(0.00)	−264.90795	(0.00)	2.92
B	−264.98893	(0.96)	−264.98625	(−0.81)	1.68					
C-11,10	−264.98928	(0.74)	−264.98598	(−0.64)	2.07	−264.91135	(0.73)	−264.91274	(−3.07)	−0.87
C-17,14	−264.98948	(0.62)	−264.98634	(−0.87)	1.97	−264.91118	(0.45)	−264.91321	(−3.36)	−0.88

[a] The designations Q; B; C-11,10; and C-17,14 stand for the geometry optimized at QCISD/6-311+G(d,p); B3LYP/6-311+G(2df,2p); CASSCF(11,10) /6-311+G(2df,2p); and CASSCF(17,14)/6-311+G(2df,2p), respectively. [b] The T_1 diagnostics are 0.0363, 0.0388, 0.0362, and 0.0362 for the CCSD wave function at QCISD, B3LYP, CASSCF(11,10), and CASSCF(17,14) geometries, respectively. [c] The T_1 diagnostics are 0.0442, 0.0435, 0.0607, and 0.0603 for the CCSD wave function at QCISD, B3LYP, CASSCF(11,10), and CASSCF(17,14) geometries, respectively.

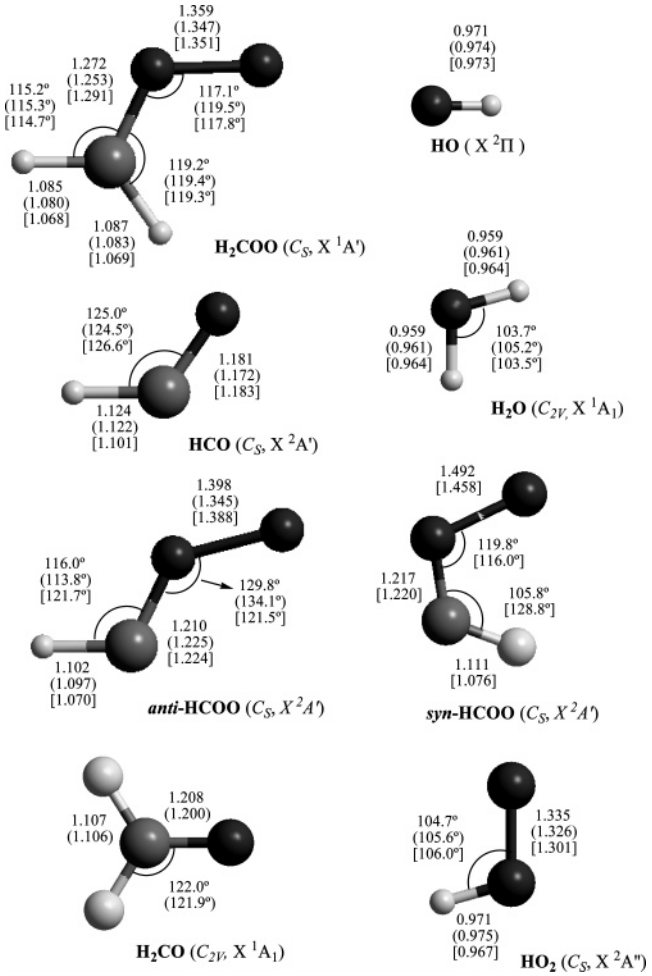

Figure 1. Selected geometrical parameters for the reactants and products, optimized at B3LYP/6-311+G(2df,2p), QCISD/6-311+G(d,p) (in brackets), and CASSCF(11,10)/6-311+G(2df,2p) (in parentheses) levels of theory.

indicate large discrepancies in the reaction energies for reaction 3 (*syn*- and *anti*-HCOO + H_2O), depending on the theoretical method employed. At this point it should be pointed out that the CCSD(T) results are unreliable as a very large T_1 diagnostic value is computed for the CCSD wave function for both HCOO isomers (T_1 diagnostic values of about 0.06, see Table S3 of Supporting Information).

Radical Addition. Table 1 and Figure 2 show that the addition of hydroxyl radical to carbonyl oxide, described by reaction 2, is the most favorable reaction path. As usual in many reactions of atmospheric interest, the process begins with the formation of a hydrogen-bonded complex (**C1**) along the reaction path, prior to the formation of the transition state (**TS1**) and the corresponding adduct $H_2C(OO)OH$ (**M1**).

Figure 3 shows that **C1** has a symmetric planar structure (C_S symmetry). Its electronic state is $^2A''$, where the unpaired electron density is orthogonal to the molecular symmetry plane and is mainly located over the oxygen of the hydroxyl radical. This complex is characterized by the electronic configuration [0.94 (...14a′^{2}1a″^{2}2a″^{2}3a″^{1}) + 0.19 (...14a′^{2}1a″^{2}3a″^{1}4a″^{2})], where the 1a″, 2a″, and 4a″ correspond to the π system of H_2COO, and consequently it maintains the biradical character of the carbonyl oxide reactant (see above). This electronic structure allows the formation of two hydrogen bonds, one of them being formed between the terminal oxygen of the carbonyl oxide moiety and the hydrogen of the hydroxyl moiety (O3H7) and the other one being formed with the *syn*-hydrogen of the H_2COO and the oxygen of HO (H4O6). The nature of such hydrogen bond interactions has been verified by a topological analysis of the corresponding wave function, performed according to the Atoms in Molecules (AIM) theory by Bader, and the values of the density and the laplacian of the density at each bond critical point are typical of hydrogen bond interactions ($\rho(r_{bcp}) = 0.0186$ e·bohr^{-3} and $\nabla^2\rho(r_{bcp}) = 0.0695$ e·bohr^{-5} for O3H7 and $\rho(r_{bcp}) = 0.0072$ e·bohr^{-3} and $\nabla^2\rho(r_{bcp}) = 0.270$ e·bohr^{-5} for H4O6). The geometrical parameters (Figure 3) computed at different levels of theory agree very well except for the bond lengths describing the hydrogen bond interactions (O3···H7 and H4···O6), which are predicted to be about 0.15 Å larger at CASSCF level of theory with respect to the QCISD optimized values. This is to be expected as the inability of the CASSCF approach to correctly describe hydrogen-bonded complexes because it cannot account correctly for the dynamical correlation effects is known. Table 1 shows that, at CCSD(T)/QCISD level of theory, **C1** is 8.15 kcal/mol more stable than the reactants (7.52 kcal/mol taking into account the BSSE corrections; Δ*E* values) and this value is reduced to 6.09 kcal/mol when the enthalpic corrections at 298 K are considered. A discussion on the relative stability of this complex at the different levels of theory employed is given below.

After **C1**, the reaction goes on through the transition state **TS1**, involving the radical addition to the carbon on the π system of carbonyl oxide. From an electronic point of view, the analysis of the CASSCF wave function at **TS1** indicates a significant contribution of several CSFs to the electronic description of the stationary point, showing an important degree of multiconfigurational character. Among them, the three most significant CSFs contributing to the wave function and their respective coefficients are as follows: [0.88 (...15a^{2}16a^{2}17a^1) − 0.20 (...15a^{2}16a^{1}17a^{1}18a^1) − 0.20 (...15a^{2}16a^{0}17a^{1}18a^2)]. The electronic features involved in this addition process are easily visualized by looking at the most significant CASSCF natural orbitals, which are displayed in Figure 4, along with their corresponding natural orbital occupation. Their analysis reveal that the addition of hydroxyl radical to carbonyl oxide involve

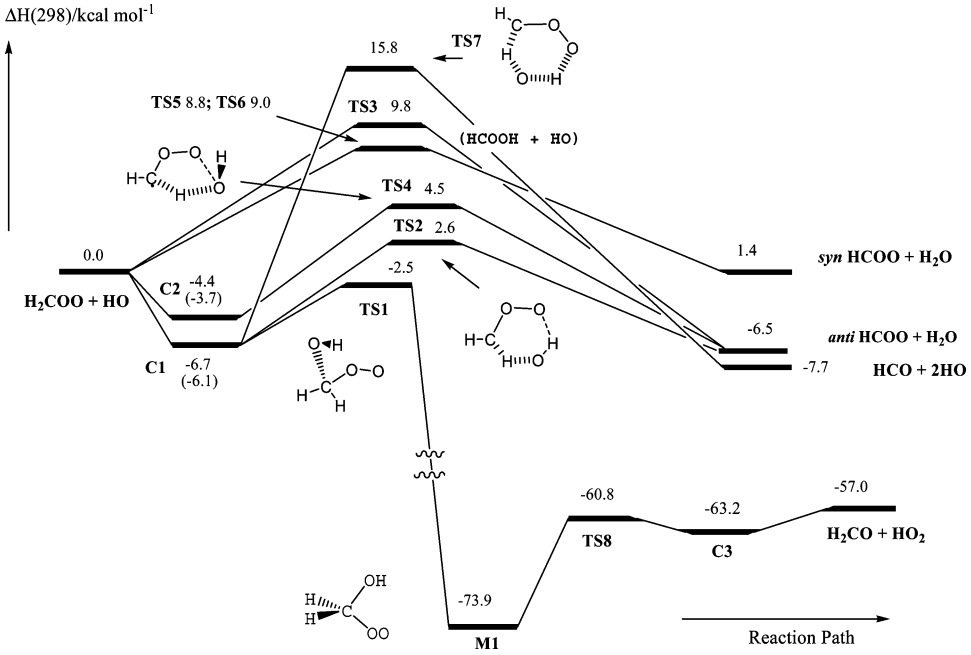

Figure 2. Schematic enthalpy diagram for the reaction between H_2COO and HO. Values in parentheses include BSSE corrections.

the unpaired electron of HO radical and the π system of H_2COO, namely, the 2a″ and 3a″ orbitals, so that the bond formation occurs by interaction of three electrons in a system of three orbitals. Regarding the geometrical parameters, the calculations carried out at QCISD and CASSCF levels of theory (see Figure 3) predict a large bond distance (about 2.32 Å) of the C1O6 bond that is being formed, which points out that this is an early transition state. This situation agrees with the fact that the corresponding CO and OO bond distances of the carbonyl oxide moiety compare with those of the reactants with differences smaller than 0.02 Å in bond distances (see also Figure 1). The remaining geometrical parameters (angles and bond lengths) computed at QCISD and CASSCF levels of theory agree within 5° and 0.04 Å, except for the H7O6C1O2 dihedral angle (see Figure 3), which differ by about 10° between QCISD and CASSCF levels. On the other side, the B3LYP approach performs worse and predicts a much larger length (2.502 Å) of the bond being formed (see Figure 3). From an energetic point of view, our results collected in Table 1 predict that, at all levels of theory considered, **TS1** lie below the separate reactants. However, we have found significant discrepancies in the computed activation energy (with respect to the **C1** complex), depending on the theoretical approach employed, which points out the difficulty of obtaining an accurate description of this elementary reaction. The origin of these discrepancies may be addressed mainly to three different factors: namely, the importance of the dynamical correlation effects in correctly describing the pre-reactive hydrogen-bonded complex; the multireferential character of the wave function; and the fact that the stationary points have been obtained and characterized at a level of theory (QCISD, B3LYP, and CASSCF) whereas the relative energies have been computed by performing single-point calculations at CCSD(T) or CASPT2 level of theory over geometries optimized with a different approach. To obtain a more accurate view on these issues, we have carried out a set of additional calculations on both **C1** and **TS1**. Thus, first we re-optimized both stationary points at CASSCF(17,14)/6-311+G(2df,2p) level of theory and then we performed additional single-point CCSD(T)/aug-cc-pVTZ and CASPT2-(17,14)/6-311+G(2df,2p) calculations on the **C1** and **TS1** geometries optimized at QCISD, B3LYP, CASSCF(11,10), and CASSCF(17,14) levels of theory, the corresponding results being displayed in Table 2. With regard to **C1**, both the CCSD(T) and CASPT2 single-point calculations indicate that the geometry optimized at QCISD level of theory has the lowest absolute energy, which lead us to conclude that this corresponds to the best geometry we have optimized from this complex. Moreover, the CCSD(T) and CASPT2 energies computed at geometries obtained by the other approaches employed differ in, at most, 0.96 kcal/mol, pointing out that **C1** has a flat potential energy surface. In addition, the corresponding values of the T_1 diagnostic of the CCSD wave function (see footnote b in Table 2) make us confident on the reliability of the energy computed at CCSD(T) level of theory and the ΔH(298K) of −6.72 kcal/mol (−6.09 kcal/mol including the BSSE correction) reported in Table 1 can be considered as the best value obtained in this work. The situation is quite different for **TS1**. Table 2 shows that the CCSD(T) energies calculated over the stationary point obtained with different approaches differ in, at most, 0.87 kcal/mol. However, the T_1 diagnostic of the corresponding CCSD wave function (with values among 0.044 and 0.061; see footnote c in Table 2) indicates important changes in the multireferential character of the wave function, making the energetic results, at least, questionable. On the other side, the single-point CASPT2 calculations show that small changes in the geometry (see Figure 3) result in large energy changes (up to 3.36 kcal/mol, see Table 2), so that the single-point CASPT2 calculations over the CASSCF optimized geometries predict energies for **TS1** lying below those computed for the pre-reactive hydrogen-bonded complex. This reflects the typical situation that arises in a very exothermic reaction having a very pronounced potential energy surface in which small changes in the geometry along the reaction coordinate involve large energy changes. These facts make it very difficult to compute an accurate prediction of the activation enthalpy for this elementary reaction. In any case, all calculations place **TS1** lying below the energy of the separate reactant. Despite this drawback, the different calculations reported in Tables 1 and 2 allow predicting of an upper limit for the **TS1**, lying 2.54 kcal/mol below the energy of the reactants (ΔH(298K) value; see Table 1).

The fate of this radical addition is the hydroxymethyl peroxy radical **M1**, $H_2C(OO)OH$, and our calculations (see Table 1 and

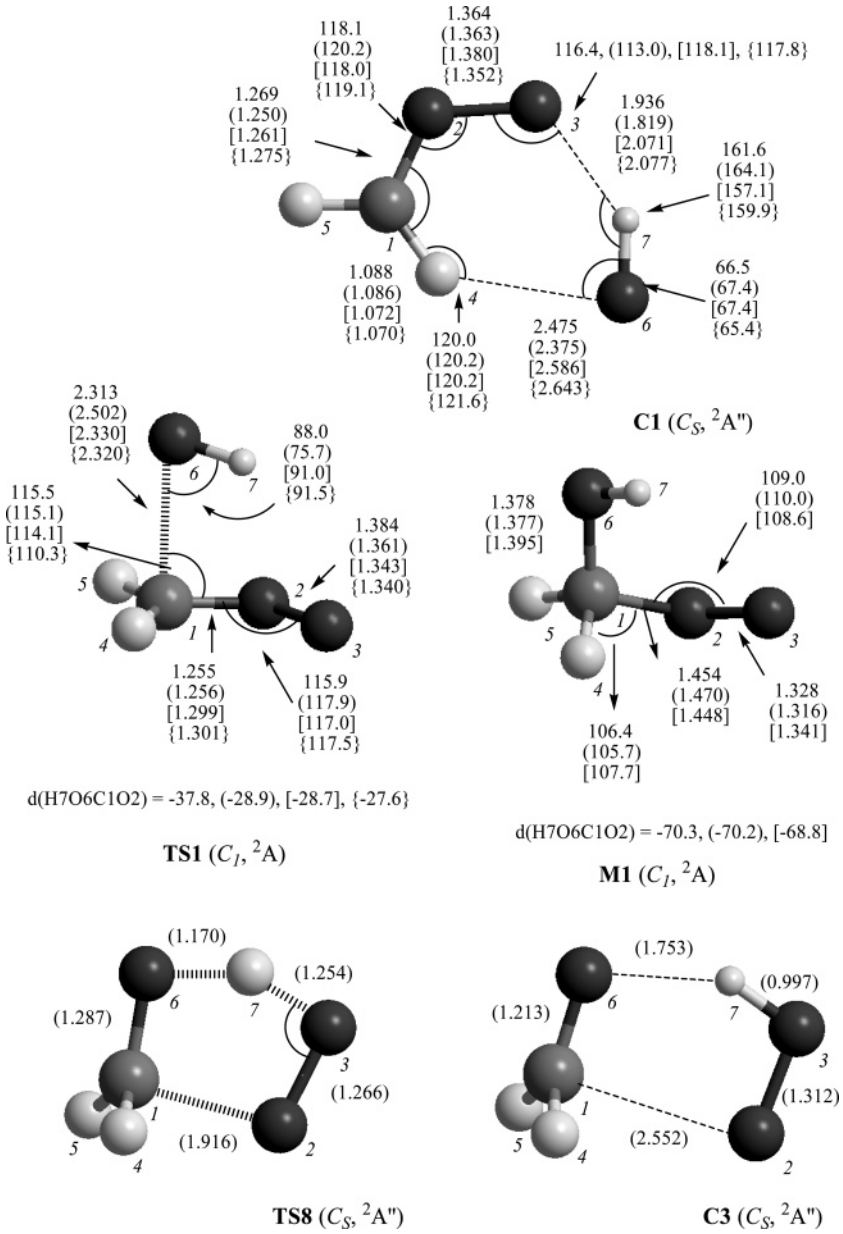

Figure 3. Selected geometrical parameters for the stationary points of the addition reaction between H_2COO and HO, optimized at B3LYP/6-311+G(2df,2p) and QCISD/6-311+G(d,p) (in parentheses), CASSCF(11,10)/6-311+G(2df,2p) (in brackets), and CASSCF(17,14)/6-311+G(2df,2p) (in claudators) levels of theory.

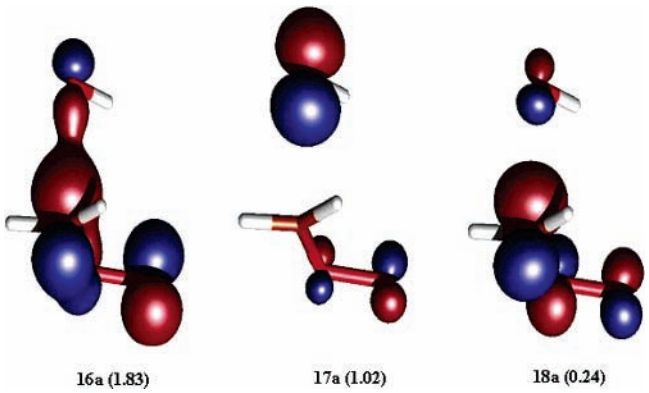

Figure 4. CASSCF natural orbitals of **TS1**, which describe the electronic features of the addition of HO to H_2COO. The corresponding natural occupation is given in parentheses.

Figure 2) predict the formation of **M1** to be exothermic by 72.9 kcal/mol relative to the separate reactants. At this point it is gratifying to observe from Table 1 that the reaction energy computed at CCSD(T) and CASPT2(17,14) levels of theory agree very well, pointing out that the CASPT2(17,14) approach accounts for the differential dynamical correlation energy in the same extent as CCSD(T) does (see the corresponding ΔE values in Table 1). The geometrical parameters of **M1** computed at different levels of theory (Figure 3) agree very well and compare also with other results reported recently in the literature for this compound.[75−78] **M1** can further decompose, producing $H_2CO + HO_2$ in a process computed to be endothermic by 16.9 kcal/mol. The corresponding reaction path has been recently reported in the literature in connection with the oxidation of the hydroxyl methyl radical by molecular oxygen[76,77] and in the reaction between formaldehyde and hydroperoxyl radical,[75,78] and we refer the reader to these references for a detailed discussion on different aspects of this process. Nevertheless, and for the sake of completeness, this decomposition profile has been included in Figure 2 and the relative energetic values have been added to Table 1, which show that the reaction goes

on through **TS8** (lying 13.1 kcal/mol above **M1**) and the hydrogen bond complex **C3** before the formation of the products. The corresponding geometries (see Figure 3) and energetic values have been taken from ref 78. Since **M1** is formed with an excess of about 73 kcal/mol, we conclude that the reaction between carbonyl oxide and hydroxyl radical will produce $H_2CO + HO_2$, the reaction being exothermic by 57 kcal/mol.

Hydrogen Abstraction. We found five reaction paths for the hydrogen abstraction of carbonyl oxide by hydroxyl radical (reaction 3). Three of them (**TS2**, **TS3**, and **TS4**) involve the abstraction of the hydrogen placed in syn (H4) of the carbonyl oxide and produces *anti*-HCOO radical and H_2O. Our calculations reveal that **TS2** possesses a symmetric six-member ring structure (Figure 5), where the hydrogen being transferred is slightly closer to hydroxyl radical (d(H4O6) = 1.143 Å) than carbonyl oxide (d(C1H4) = 1.375 Å). The corresponding electronic state is $^2A'$ and is mainly characterized by the $13a'^2 3a''^2 14a'^1$ electronic configuration, which describes the concerted breaking and making of the C1···H4 and H4···O6 bonds, respectively; that is, the mechanism corresponds to the conventional *hydrogen transfer mechanism* expected from radical chemistry. In addition, Figure 1 shows also that, at **TS2**, the distance between the hydrogen of the HO radical and the terminal oxygen of carbonyl oxide (O3···H7) is about 2 Å, suggesting the presence of a hydrogen bond interaction. This hydrogen bond interaction has been confirmed by performing a topological analysis of the corresponding wave function ($\rho(r_{bcp}) = 0.0146$ e·bohr^{-3} and $\nabla^2\rho(r_{bcp}) = 0.0553$ e·bohr^{-5}) and produces a stabilization effect. Figure 2 shows that this process begins with the formation of the pre-reactive **C1** complex (discussed above). From an energetic point of view, the results displayed in Table 1 indicate that the ΔE values obtained at all levels of theory agree quite well (about 4.9 kcal/mol above the reactants).

The elementary reaction path occurring through **TS3** has the same electronic features as those described for **TS2**; that is, the process involves a conventional hydrogen atom transfer mechanism. However, in this case the hydroxyl radical approaches H4 in trans with respect to the COO group, leading to a nonsymmetrical structure for the transition state. The corresponding geometrical parameters displayed in Figure 5 indicate that the hydrogen being transferred is closer to the hydroxyl radical (d(H4O6) = 1.185 Å) than carbonyl oxide (d(C1H4) = 1.276 Å), the carbon atom is slightly piramidalized (with an OOCH4 dihedral angle of about 44°), and consequently, the CO bond has been enlarged considerably (d(CO) = 1.370 Å). For this process we have computed a barrier height of 9.77 kcal/mol relative to the separate reactants, which is significantly higher than the 2.59 kcal/mol computed for **TS2** and having the same electronic features with respect to the hydrogen abstraction process. These results point out the importance of the hydrogen bond interaction and allow us to quantify its stabilization effect, which is on the order of 7 kcal/mol.

For the reaction path taking place through **TS4** we have computed a barrier height of 4.53 kcal/mol relative to the separate reactants (ΔH(298K) value) and it is very interesting from an electronic point of view. Here, the hydroxyl radical approaches carbonyl oxide with the HO outside the plane defined by the carbonyl oxide moiety, in such a way that the unpaired electron interacts with the terminal oxygen of H_2COO whereas a lone pair of the oxygen of the HO moiety faces H4 of carbonyl oxide. The resulting transition structure (**TS4**, see Figure 1) has a five-member ring structure where the hydrogen being transferred is halfway between C1 and O6 (d(C1H4) = 1.305 Å and d(H4O6)=1.273 Å) and an interaction between O3···O6 has been identified in the ring structure by the AIM topological analysis ($\rho(r_{bcp}) = 0.0576$ e·bohr^{-3} and $\nabla^2\rho(r_{bcp}) = 0.2399$ e·bohr^{-5}). Moreover, the analysis of the CASSCF wave function along with the analysis of the atomic spin population show that the unpaired electron is shared between O6 and O3, which indicates that this interaction leads to a process that involves the transfer of an electron from a lone pair of the terminal oxygen of the H_2COO moiety to the oxygen of the HO radical, coupled with the H4 proton shift to the oxygen of the hydroxyl radical, that is, a *proton coupled electron-transfer mechanism* (*pcet*). The same kind of interaction was recently described in the literature for the gas oxidation of formic acid by hydroxyl radical,[79,80] but here it is worth pointing out that the proton being transferred is linked to the carbon of H_2COO in the reactant. Figure 2 shows that the reaction begins with a pre-reactive hydrogen-bonded complex **C2**, whose geometrical structure has been displayed in Figure 3. The complex already presents the five-member ring structure as does **TS4**, where both moieties are held together by an H4···O6 hydrogen bond interaction and by an O3···O6 interaction. At this point it must be pointed out that **C2** was found only at B3LYP level of theory while any attempt we performed with the other theoretical approaches employed converged to **C1**. The reason for this is that at B3LYP level of theory **C2** is the most stable complex whereas at QCISD or CASSCF levels **C1** lies below in energy so the optimization procedure converges to **C1**. A similar situation was found in the study of the complexes formed between HCOOH and HO, where the same kind of interactions as those described here was reported.[81] From an energetic point of view, the results of Table 1 predict **C2** to be more stable than the reactants by 4.42 kcal/mol (3.71 kcal/mol considering the BSSE corrections; ΔH(298K) value) and these results indicate also that **C2** is placed 2.3 kcal/mol above **C1** according to the calculations computed at the best level of treatment employed.

The remaining two transition states (**TS5** and **TS6**) involve the abstraction of the hydrogen placed in anti (H5) of the H_2COO, leading to the formation of *syn*-HCOO radical and H_2O. Both transition states are conformers that differ from each other in the relative orientation of the HO moiety (in cis or trans, respectively), with respect to the COO group. In both cases, the reaction involves the conventional hydrogen (H5) atom abstraction and has the same electronic and geometric features as discussed above for **TS3**. Accordingly, the corresponding activation barriers are very similar, about 9 kcal/mol relative to the separate reactants (see Table 1 and Figure 2).

Double Proton Transfer. Figures 2 and 3 show that the process occurring through **TS7** involves the transfer of H4 of carbonyl oxide to the oxygen of the hydroxyl radical, simultaneously with the transfer of the hydrogen of the HO to the terminal oxygen of the H_2COO. The reaction path begins with the formation of the complex **C1** (discussed above) and goes on through **TS7** and its fate is the formation of HCO radical plus two molecules of hydroxyl radical (reaction 4). From an electronic point of view, **TS7** has the same symmetry and electronic description as **C1** (C_S symmetry, $^2A''$, $14a'^2 2a''^2 3a''^1$), which imply that, along all of the reaction path, the unpaired electron density is perpendicular to the molecular symmetry plane, and mainly located over the oxygen of the hydroxyl radical. Consequently, the radical does not take place in the reaction and the process involves a *double proton transfer (dpt)*. That is, H4 moves from the carbon to the oxygen of the hydroxyl

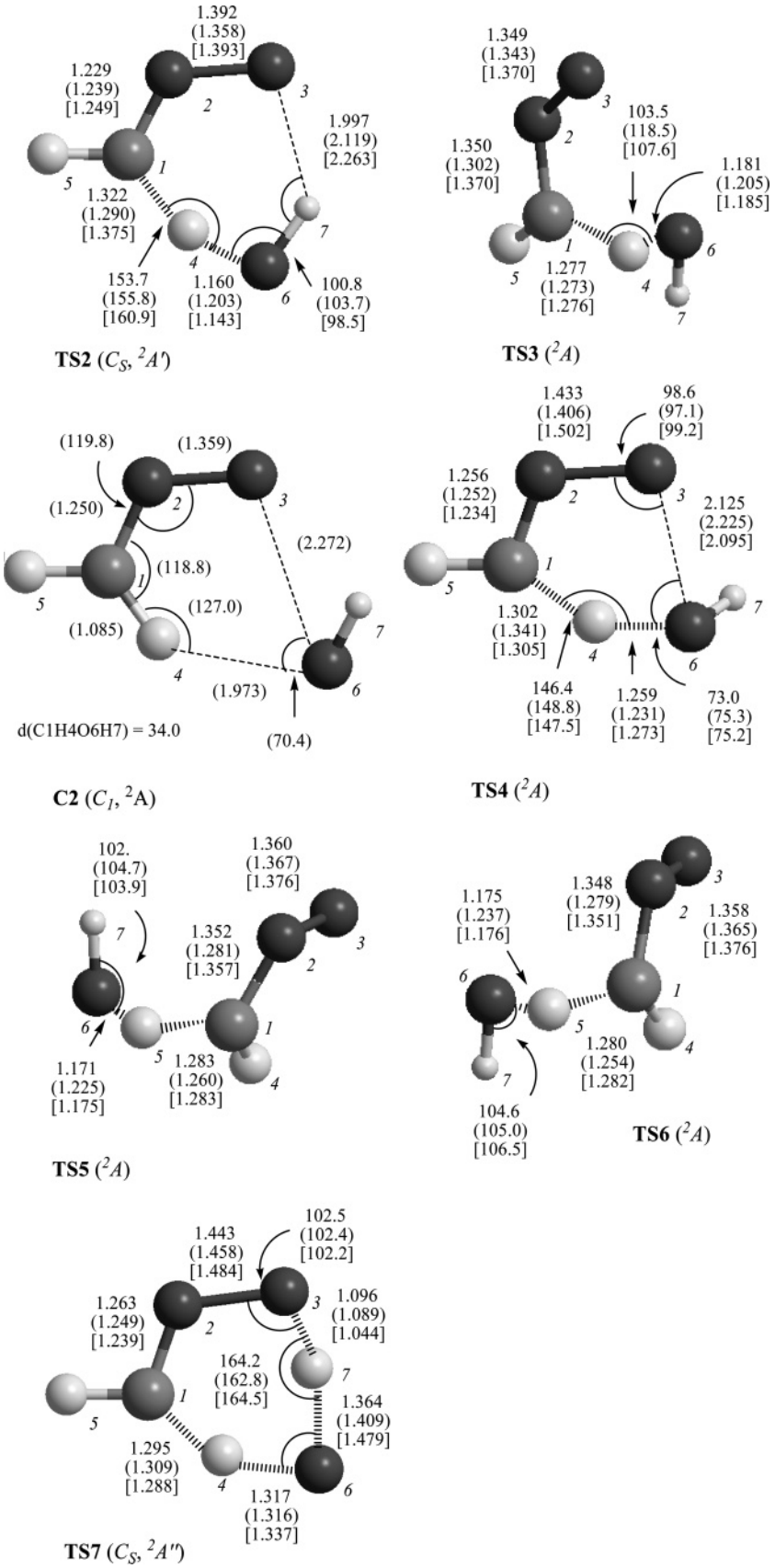

Figure 5. Selected geometrical parameters for the stationary points of the hydrogen abstraction reaction and double proton transfer process between H_2COO and HO, optimized at B3LYP/6-311+G(2df,2p), QCISD/6-311+G(d,p) (in parentheses), and CASSCF(11,10)/6-311+G(2df,2p) (in brackets) levels of theory.

radical and simultaneously H7 moves from the oxygen of HO radical to the terminal oxygen of carbonyl oxide. Thus, the double proton transfer process occurring through **TS7** produces, in a first step, HC(OOH) plus HO radical and the HC(OOH) intermediate decomposes into HCO + OH. The formation of HC(OOH) and its decomposition has been reported in the

SCHEME 1: Mechanism of the Reaction between H_2COO with HO and Pictorial Representation of the Corresponding Electronic Features

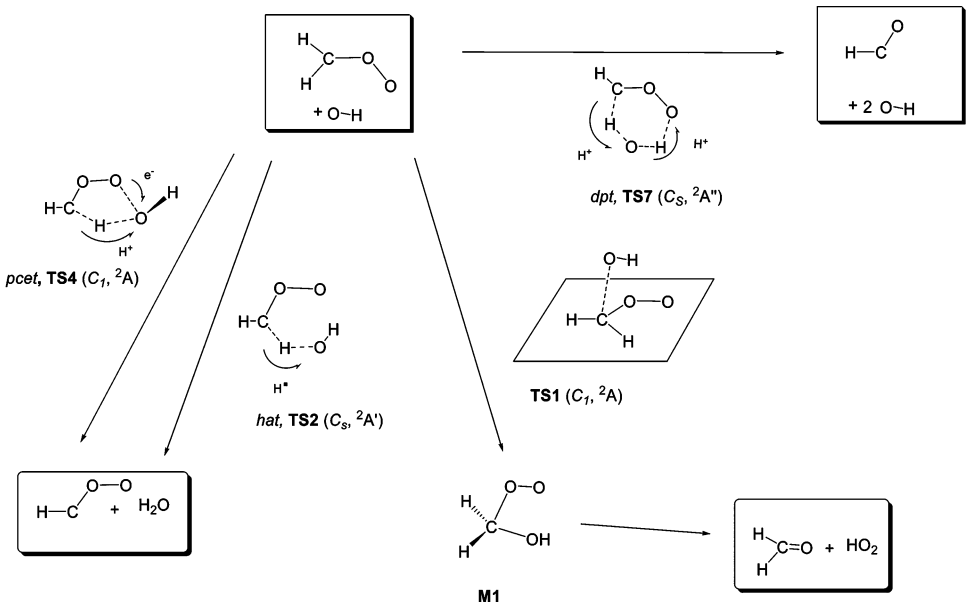

literature by Gutbrod and co-workers,[27] and we refer the reader to this reference for a more detailed discussion on this process.

Electronically, this *dpt* reaction is similar to the double proton transfer described recently in the reaction of HCOOH + HO,[80] where the acidic proton is transferred to the oxygen of HO radical and simultaneously the proton of the radical is transferred to the oxygen of the carbonyl group producing a silent reaction. Moreover, the process is very similar to the hydrogen transfer process described in the reaction between carbonyl oxide and water, leading to HC(OOH) + H_2O. In that work, H_2O acts as a catalyst of the equivalent intermolecular hydrogen transfer reported by Gutbrod and co-workers[27] for H_2COO, and the same catalytic role is played here by HO radical. This catalytic effect can be seen comparing the barrier height reported by Gutbrod and co-workers (ΔH(298K) = 30.8 kcal/mol) for the unimolecular process $H_2COO \rightarrow HCO + HO$[27] with the barrier height relative to the reactants (ΔH(298K) = 11.9 kcal/mol) for $H_2COO + H_2O \rightarrow HCO + HO + H_2O$ reported in the literature[36,37] and with the barrier height relative to the reactants of the reaction described in this work (ΔH(298K) = 15.8 kcal/mol, see Table 1) for $H_2COO + HO \rightarrow HCO + 2HO$.

Summary and Conclusions

The principal trends of the mechanism of the gas-phase reaction between carbonyl oxide and hydroxyl radical are summarized in Scheme 1, which also includes a pictorial diagram of the electronic features involved in the different elementary processes. From an electronic point of view, we have identified four different kinds of processes: namely, the radical addition (*rad*) to the carbon, on the π system of carbonyl oxide; a hydrogen atom abstraction (*hat*) by HO radical in which a hydrogen atom from carbonyl oxide is transferred to the oxygen of the radical; a process involving a proton coupled electron-transfer mechanism (*pcet*), where the oxygen of the hydroxyl radical abstracts the proton placed in syn on the carbonyl oxide and simultaneously an electron from the terminal oxygen of the H_2COO is transferred to the oxygen of HO; and a double proton transfer mechanism (*dpt*), where the HO radical acts as a catalyst in an intermolecular transfer of the hydrogen linked in syn of the carbonyl oxide to the terminal oxygen. In more detail, our investigation on this reaction, reported in the present work, led us to the following:

(1) The most favorable reaction path involves the addition of the HO radical to the carbon of the carbonyl oxide, which leads to the formation of the peroxy radical $H_2C(OO)OH$ (**M1**) in a reaction computed to be exothermic by 72.9 kcal/mol. As usual in many reactions of interest in atmospheric chemistry, the reaction between H_2COO and HO begins with the formation of a hydrogen-bonded complex (**C1**), prior to the transition state **TS1**, so this is not an elementary reaction but a complex process. **C1** lies 6.09 kcal/mol below the sum of the enthalpies of the reactants and is stabilized by two hydrogen bonds and **TS1** is computed to lie 2.54 kcal/mol below the reactants (ΔH(298K) value).

(2) Recent results reported in the literature show that the peroxy radical **M1** can decompose, producing $H_2CO + HO_2$ in a process being endothermic by about 17 kcal/mol. Since **M1** is formed with an excess of about 73 kcal/mol, we can conclude that the reaction between H_2COO and HO will produce formaldehyde and hydroperoxy radical, according to reaction 2.

(3) We have found five reaction paths (**TS2**, **TS3**, **TS4**, **TS5**, and **TS6**), involving the abstraction of a hydrogen of carbonyl oxide, that lie energetically among 2.6 and 9.0 kcal/mol above the sum of the enthalpies of the reactants (reaction 3). Of special interest from a mechanistic point of view are the processes through **TS2** and **TS4**. **TS2** involves a hydrogen atom transfer mechanism (*hat*), but it is additionally stabilized by a hydrogen bond, whereas the elementary reaction through **TS4** involves an unexpected proton coupled electron transfer mechanism (*pcet*).

(4) We found a reaction path (**TS7**), lying 15.8 kcal/mol above the sum of the enthalpies of the reactants, involving a double proton transfer process in which the hydrogen in syn of the H_2COO moves to the oxygen of the HO radical and simultaneously the hydrogen of the hydroxyl radical is transferred to the terminal oxygen of the carbonyl oxide in a process where the HO radical acts as a catalyst.

(5) The low activation enthalpy computed for **TS1** in relation to the other processes considered suggest that, in the gas phase,

only the addition process will take place. However, the mechanistic knowledge of the remaining processes investigated may be of interest for the study of reactions involving substituted carbonyl oxides or for the study of the reaction in solution.

Acknowledgment. The financial support for this research was provided by the Spanish Dirección General de Investigación Científica y Técnica (DGYCIT, Grant CTQ2005-07790) and by the Generalitat de Catalunya (Grant 2005SGR00111). The calculations described in this work were carried out at the Centre de Supercomputació de Catalunya (CESCA) and the Centro de Supercomputación de Galicia (CESGA), whose services are gratefully acknowledged, and at an AMD Opteron cluster of our group. A. Mansergas thanks the Spanish Ministerio de Educación y Ciencia for a fellowship (BES-2003-1352).

Supporting Information Available: Absolute energy values; topological parameters of selected stationary points; Cartesian coordinates of the stationary points reported in this work; and a schematic description of the active space composition used for the CASSCF calculations. This material is available free of charge via the Internet at http://pubs.acs.org.

References and Notes

(1) Wayne, R. P. *Chemistry of Atmospheres*, 3rd ed.; Oxford University Press: Oxford, 2000.
(2) Atkinson, R.; Aschmann, S. M.; Arey, J.; Shorees, B. *J. Geophys. Res.* **1992**, *97*, 6065.
(3) Atkinson, R.; Aschmann, S. M. *Environ. Sci. Technol.* **1993**, *27*, 1357.
(4) Paulson, S. E.; Orlando, J. J. *Geophys. Res. Lett.* **1996**, *23* (25), 3727.
(5) Paulson, S. E.; Sen, A. D.; Liu, P.; Fenske, J. D.; Fox, M. J. *Geophys. Res. Lett.* **1997**, *24* (24), 3193.
(6) Pfeiffer, T.; Forberich, O.; Comes, F. J. *Chem. Phys. Lett.* **1998**, *298*, 3251.
(7) Donahue, N.; Kroll, J. H.; Anderson, J. G. *Geophys. Res. Lett.* **1998**, *25* (1), 59.
(8) Paulson, S. E.; Chung, M. Y.; Hasson, A. S. *J. Phys. Chem. A* **1999**, *103* (41), 8127.
(9) Paulson, S. E.; Fenske, J. D.; Sen, A. D.; Callahan, T. W. *J. Phys. Chem. A* **1999**, *103*, 2050.
(10) Neeb, P.; Moortgat, G. K. *J. Phys. Chem. A* **1999**, *103*, 9003.
(11) Mihelcic, D.; Heitlinger, M.; Kley, D.; Müsgen, P.; Volz-Thomas, A. *Chem. Phys. Lett.* **1999**, *301*, 559.
(12) Lewin, A. G.; Johnson, D.; Price, D. W.; Marston, G. *Phys. Chem. Chem. Phys.* **2001**, *3*, 1253.
(13) Kroll, J. H.; Clarke, J. S.; Donahue, N. M.; Anderson, J. G.; Demerjian, K. L. *J. Phys. Chem. A* **2001**, *105*, 1554.
(14) Paulson, S. E.; Flagan, R. C.; Seinfeld, J. H. *Int. J. Chem. Kinet.* **1992**, *24*, 103.
(15) Zhang, D.; Lei, W.; Zhang, R. *Chem. Phys. Lett.* **2002**, *358*, 171.
(16) Zhang, D.; Zhang, R. *J. Am. Chem. Soc.* **2002**, *124* (11), 2692.
(17) Criegee, R. *Angew. Chem., Int. Ed.* **1975**, *14* (11), 745.
(18) Su, F.; Calvert, G.; Shaw, H. H. *J. Phys. Chem.* **1980**, *84*, 239.
(19) Horie, O.; Moortgat, G. K. *Atmos. Environ.* **1991**, *25A*, 1881.
(20) Atkinson, R. *J. Phys. Ref. Data* **1997**, *26*, 215.
(21) Neeb, P.; Horie, O.; Moortgat, G. K. *J. Phys. Chem. A* **1998**, *102*, 6778.
(22) Horie, O.; Mortgat, G. K. *Acc. Chem. Res.* **1998**, *31*, 387.
(23) Herron, J. T.; Huie, E. *J. Am. Chem. Soc.* **1977**, *99* (16), 5430.
(24) Niki, H.; Maker, P. D.; Savage, C. M.; Breitenbach, L. P.; Hurley, M. D. *J. Phys. Chem.* **1987**, *91*, 941.
(25) Martinez, R. I.; Herron, J. T. *J. Phys. Chem.* **1988**, *92*, 4644.
(26) Cremer, D.; Gauss, J.; Kraka, E.; Stanton, J. F.; Bertlett, R. J. *Chem. Phys. Lett.* **1993**, *209*, 547.
(27) Gutbrod, R.; Schindler, R. N.; Kraka, E.; Cremer, D. *Chem. Phys. Lett.* **1996**, *252*, 221.
(28) Gutbrod, R.; Kraka, E.; Schindler, R. N.; Cremer, D. *J. Am. Chem. Soc.* **1997**, *119*, 7330.
(29) Anglada, J. M.; Bofill, J. M.; Olivella, S.; Solé, A. *J. Am. Chem. Soc.* **1996**, *118* (19), 4636.
(30) Anglada, J. M.; Bofill, J. M.; Olivella, S.; Solé, A. *J. Phys. Chem. A* **1998**, *19*, 3398.
(31) Anglada, J. M.; Crehuet, R.; Bofill, J. M. *Chem.-Eur. J.* **1999**, *5* (6), 1809.
(32) Becker, K. H.; Barnes, I.; Ruppert, L.; Wiesen, P. Free Radicals in the Atmosphere: The Motor of Tropospheric Oxidation Processes. In *Free Radicals in Biology and Environment*; Minisci, F., Ed.; Kluwer Academic Publishers: Dordrecht, 1996; p 365.
(33) Hatakeyama, S.; Akimoto, H. *Res. Chem. Intermed.* **1994**, *20*, 503.
(34) Horie, O.; Neeb, P.; Moortgat, G. K. *Int. J. Chem. Kinet.* **1997**, *29*, 461.
(35) Fenske, J. D.; Hasson, A. L.; Ho, A. W.; Paulson, S. E. *J. Phys. Chem. A* **2000**, *104*, 9921.
(36) Crehuet, R.; Anglada, J. M.; Bofill, J. M. *Chem.-Eur. J.* **2001**, *7* (10), 2227.
(37) Anglada, J. M.; Aplincourt, P.; Bofill, J. M.; Cremer, D. *ChemPhysChem* **2002**, *2*, 215.
(38) Hasson, A. S.; Chung, M. Y.; Kuwata, K. T.; Converse, A. D.; Krohn, D.; Paulson, S. E. *J. Phys. Chem. A* **2003**, *107* (32), 6176.
(39) Aplincourt, P.; Anglada, J. M. *J. Phys. Chem. A* **2003**, *107*, 5798.
(40) Orzechowska, G.; Paulson, S. E. *J. Phys. Chem. A* **2005**, *109* (24), 5358.
(41) Mansergas, A.; Anglada, J. M., unpublished work.
(42) Roos, B. O. *Adv. Chem. Phys.* **1987**, *69*, 399.
(43) Hariharan, P. C.; Pople, J. A. *Theor. Chim. Acta* **1973**, *28*, 213.
(44) Frisch, M. J.; Pople, J. A.; Binkley, J. S. *J. Chem. Phys.* **1984**, *80*, 3265.
(45) Hehre, W. J.; Radom, L.; Schleyer, P. v. R.; Pople, J. A. In *Ab Initio Molecular Orbital Theory*; John Wiley: New York, 1986; p 86.
(46) Anglada, J. M.; Bofill, J. M. *Chem. Phys. Lett.* **1995**, 243, 151.
(47) Buenker, R. J.; Peyerimhoff, S. D. *Theor. Chim. Acta* **1975**, *39*, 217.
(48) Buenker, R. J.; Peyerimhoff, S. D. In *New Horizons of Quantum Chemistry*; Lowdin, P. O., Pullman, B., Eds.; D. Reidel: Dordrecht, The Netherlands, 1983; Vol. 35, p 183.
(49) Buenker, R. J.; Philips, R. A. *J. Mol. Struct.: THEOCHEM* **1985**, *123*, 291.
(50) Becke, A. D. *J. Chem. Phys.* **1993**, *98*, 5648.
(51) Ishida, K.; Morokuma, K.; Kormornicki, A. *J. Chem. Phys.* **1977**, *66*, 2153.
(52) Gonzalez, C.; Schlegel, H. B. *J. Chem. Phys.* **1989**, *90*, 2154.
(53) Gonzalez, C.; Schlegel, H. B. *J. Phys. Chem.* **1990**, *94*, 5523.
(54) Pople, J. A.; Head-Gordon, M.; Raghavachari, *J. Chem. Phys.* **1987**, *87*, (10), 5968.
(55) Pople, J. A.; Krishnan, R.; Schlegel, H. B.; Binkley, J. S. *Int. J. Quantum Chem. XIV* **1978**, 545.
(56) Cizek, J. *Adv. Chem. Phys.* **1969**, *14*, 35.
(57) Barlett, R. J. *J. Phys. Chem.* **1989**, *93*, 1963.
(58) Raghavachari, K.; Trucks, G. W.; Pople, J. A.; Head-Gordon, M. *Chem. Phys. Lett.* **1989**, *157*, 479.
(59) Dunning, T. H. J. *J. Chem. Phys.* **1989**, *90*, 1007.
(60) Kendall, R. A.; Jr. Dunning, T. H.; Harrison, R. J. *Chem. Phys* **1992**, 6769.
(61) Lee, T. J.; Taylor, P. R. *T1 Diag. Int. J. Quantum Chem. Symp.* **1989**, *23*, 199.
(62) Rienstra-Kiracofe, J. C.; Allen, W. D.; Schaefer, H. F., III. *J. Phys. Chem. A* **2000**, *104*, 9823.
(63) Boys, S. F.; Bernardi, F. *Mol. Phys.* **1970**, *19*, 553.
(64) Frisch, M. J.; Trucks, G. W.; Schlegel, H. B.; Scuseria, G. E.; Robb, M. A.; Cheeseman, J. R.; Zakrzewsk, V. G.; Montgomery, J. A.; Stratmann, R. E.; Buran, J. C.; Dapprich, S.; Millam, J. M.; Daniels, A. D.; Kudin, K. N.; Strain, M. C.; Farkas, O.; Tomasi, J.; Barone, V.; Cossi, M.; Cammi, R.; Mennucci, B.; Pomelli, C.; Adamo, C.; Clifford, S.; Ochterski, J.; Petersson, G. A.; Ayala, P. Y.; Cui, Q.; Morokuma, K.; Rega, N.; Salvador, P.; Dannenberg, J. J.; Malick, D. K.; Rabuck, A. D.; Raghavachari, K.; Foresman, J. B.; Cioslowski, J.; Ortiz, V.; Baboul, A. G.; Stefanov, B. B.; G. Liu, A. L.; Piskorz, P.; Komaromi, I.; Martin, R. G. L.; Fox, D. J.; Keith, T.; Al-Laham, M. A.; Peng, C. Y.; Nanayakkara, A.; Challacombe, M.; Gill, P. M. W.; Johnson, B.; W. Chen, M. W. W.; Andres, J. L.; Gonzalez, C.; Head-Gordon, M.; Replogle, E. S.; Pople, J. A. *Gaussian 98, Revision A.11*; Gaussian, Inc.: Pittsburgh, PA, 2002.
(65) Schmidt, M. W.; Baldrige, K. K.; Boatz, J. A.; Elbert, S. T.; Gordon, M. S.; Jensen, J. H.; Koseki, S.; Matsunaga, N.; Nguyen, K. A.; Su, S. J.; Windus, T. L.; Duouis, M.; Montgomery, J. A. *J. Comput. Chem.* **1993**, *14*, 134.
(66) Andersson, K.; Barysz, M.; A., B.; A., B. M. R.; Cooper, D. L.; Fleig, T.; Fülscher, M. P.; DeGraaf, C.; Hess, B. A.; Karlström, G.; Lindh, R.; Malmqvist, P.-Å. N., P.; Olsen, J.; Roos, B. O. S., A. J.; Schütz, M.; Schimmelpfennig, B.; Seijo, L.; Serrano-Andrés, L. S., P. E. M.; Stålring, J.; Thorsteinsson, T.; Veryazov, V. W., P. O *MOLCAS*, version 5; Lund University, 2000.
(67) Shaftenaar, G.; Noordik, J. H. *J. Comput.-Aided Mol. Des.* **2000**, *14*, 123.
(68) Bader, R. F. W. *Atoms in Molecules. A Quantum Theory*; Clarendon Press: Oxford, 1995; Vol. 22.
(69) Bader, R. F. W. *AIMPAC*; http://www.chemistry.mcmaster.ca/aimpac, downloaded May 2002.

(70) Olzmann, M.; Kraka, E.; Cremer, D.; Gutbrod, R.; Andersson, S. *J. Phys. Chem.* **1997**, *101*, 9421.
(71) Bach, R. D.; Owensby, A. L.; Andrés, J. L.; Schlegel, H. B. *J. Am. Chem. Soc.* **1991**, *113*, 7031.
(72) Crehuet, R.; Anglada, J. M.; Cremer, D.; Bofill, J. M. *J. Phys. Chem. A* **2002**, *106* (15), 3917.
(73) Chen, B.-Z.; Anglada, J. M.; Huang, M.-B.; Kong, F. *J. Phys. Chem. A* **2002**, *106* (9), 1877.
(74) Huang, M.-B.; Chen, B.-Z.; Wang, Z.-X. *J. Phys. Chem. A* **2002**, *106* (22), 5490.
(75) Evleth, E. M.; Melius, J. C. F.; Rayez, M. T.; Rayez, J. C.; Forsts, W. *J. Phys. Chem.* **1993**, *97*, 5040.
(76) Olivella, S.; Bofill, J. M.; Solé, A. *Chem.-Eur. J.* **2001**, *7*, 3377.
(77) Dibble, T. S. *Chem. Phys. Lett.* **2002**, *355*, 193.
(78) Anglada, J. M.; Domingo, V. M. *J. Phys. Chem. A* **2005**, *109*, 10786.
(79) Olivella, S.; Anglada, J. M.; Sole, A.; Bofill, J. M. *Chem.-Eur. J.* **2004**, *10*, 3404.
(80) Anglada, J. M. *J. Am. Chem. Soc.* **2004**, *126*, 9809.
(81) Torrent-Sucarrat, M.; Anglada, J. M. *ChemPhysChem* **2004**, *5*, 183.